

# Testing the random field model hypothesis for random marked closed sets

Antonín Koubek<sup>a</sup>, Zbyněk Pawlas<sup>a</sup>, Tim Brereton<sup>b</sup>, Björn Kriesche<sup>b</sup>,  
Volker Schmidt<sup>b</sup>

<sup>a</sup>*Department of Probability and Mathematical Statistics, Faculty of Mathematics and Physics, Charles University in Prague, Sokolovská 83, 18675 Praha 8, Czech Republic*

<sup>b</sup>*Institute of Stochastics, Ulm University, 89069 Ulm, Germany*

---

## Abstract

When developing statistical models, it is of fundamental importance to decide if the various components are independent of one another, preferably using a formal statistical test. Non-parametric versions of such tests are particularly useful, as they do not require extensive *a priori* knowledge about the underlying models. In this paper, we develop such tests for random marked closed sets, which have many applications in spatial statistics. More precisely, we investigate two approaches to testing if the marks are independent of the closed set. Both approaches are based on second-order characteristics of random marked closed sets. The first approach uses a global rank envelope test based on the mark-weighted  $K$ -function. The second approach uses an asymptotic test developed for marked point processes. We carry out extensive simulation studies to assess the performance of these tests, demonstrating that the global rank envelope test is a better choice. Finally, we apply this test to two real world data sets.

*Keywords:* random marked closed set, random field model, envelope test, subsampling, Monte Carlo test, mark-weighted  $K$ -function

---

## 1. Introduction

The notion of a *random marked closed set* (RMCS) is defined in [2] as a random upper semi-continuous function on a random domain (random closed set). Many settings in spatial statistics are naturally described by RMCSs. For example, the closed set could represent forest areas and the mark function could express the local stand density, or the closed set could represent bodies

of water and the mark function could represent water quality. In [22], RMCSs are used to investigate metallic materials, with the grain boundary network being represented by a random set marked by the disorientation angles of the grain boundaries.

Marked point processes are special examples of RMCSs. They are used to model spatial data that consist of measurements at irregularly scattered spatial locations; see, e.g., [5], [6] and [9]. The locations are treated as a realization of a spatial point process (which is a particular example of random closed set) and the associated measurements are treated as the corresponding marks. In practice, the points and the marks are often correlated. For instance, in forestry data, the points (representing tree locations) and marks (representing tree size) could be correlated; see, e.g., the examples in [21]. A critical task when developing a statistical model of a marked point process is to determine if the values of the marks are independent of the locations of the corresponding points.

The simplest model of a marked point process is an independently marked (or randomly labeled) point process, where the marks are i.i.d. and independent of the points. In order to model correlated marks, Karr [11] considered marks generated by a random field that is independent of the points. Such marking is called *geostatistical marking* and the corresponding marked point process model is called a *random field model*; cf. [9, Section 5.1.3] and [19]. Several methods have been proposed for testing the hypothesis that a marked point process has independent marks; see [9, Section 7.5.2], [16]. Tests have also been proposed for determining if a stationary marked point process follows the random field model; see [7], [8], [9, Section 7.5.3], [19], [24].

A natural generalization of a marked point process is to consider the labeling of random closed sets. These are studied in [15], where the connected components of the set are labeled by nominal marks. Labeled random closed sets are also studied in [18], where they are used to model multi-phase data, representing the presence of different sulphides in an ore sample. In [1], where the random closed set only has two possible marks (representing degenerated and normal nerve fibre) a test is introduced to determine if the marks are mutually independent and independent of the set.

The notion of a RMCS further generalizes both marked point processes and labeled random closed sets. A fundamental question when using a RMCS to model data is whether the marks are independent of the domain. This situation is an analogue of the random field model for marked point processes. If the random field model hypothesis is satisfied, then the statistical analysis

of the RMCS is simplified considerably, since the two components may be investigated separately. If it is not satisfied, then care must be taken to adequately model the nature of the dependency.

In general, when working with data that is assumed to come from a RMCS, little is known *a priori* about the random marks and the random closed set. Indeed, an important application of a test of the random field hypothesis is to determine whether the random marks and random closed set can be studied and modeled separately of one another. Thus, it is important to develop tests that do not rely on detailed knowledge about the models from which the random marks and random closed set come. For this reason, in this paper, we develop two non-parametric tests of the random field model hypothesis. Both approaches are based on second-order characteristics of RMCSs. The first test is a global rank envelope test (see [17]) based on the mark-weighted  $K$ -function. In order to apply this test, a set of test points needs to be carefully chosen. The second test overlays the random set with an independent point process and then uses a test developed for marked point processes in [8]. We carry out simulations to assess the performance of these tests. These simulations suggest that the global rank envelope test performs best. Finally, we apply our methodology to real world radar data on adjusted hourly precipitation in Germany and to microscopic image data showing the nanostructure of a thin film organic semiconductor.

## 2. Random marked closed sets

Consider the space

$$\Phi_{\text{usc}} = \{(X, f) : X \subseteq \mathbb{R}^d \text{ is closed, } f : X \rightarrow \bar{\mathbb{R}} \text{ is upper semi-continuous}\},$$

where  $\bar{\mathbb{R}} = \mathbb{R} \cup \{-\infty, \infty\}$ . A RMCS,  $(\Xi, \Gamma)$ , in  $\mathbb{R}^d$  is defined in [2] as a random element in  $\Phi_{\text{usc}}$ . More precisely,  $(\Xi, \Gamma)$  is a mapping from an abstract probability space  $(\Omega, \mathcal{A}, \mathbb{P})$  to  $\Phi_{\text{usc}}$  such that, for every compact set  $K$  in  $\mathbb{R}^d \times \bar{\mathbb{R}}$ ,

$$\{\omega \in \Omega : \tau((\Xi, \Gamma)(\omega)) \cap K \neq \emptyset\} \in \mathcal{A},$$

where  $\tau(X, f) = \{(x, t) \in X \times \bar{\mathbb{R}} : t \leq f(x)\}$  is a closed set in  $\mathbb{R}^d \times \bar{\mathbb{R}}$ . In other words, a RMCS,  $(\Xi, \Gamma)$ , can be understood as a random upper semi-continuous function,  $\Gamma$ , defined on a random closed set,  $\Xi$ . The domain,  $\Xi$ , is a random element with values in the space of all closed subsets of  $\mathbb{R}^d$ . We refer to  $\Gamma$  as the mark field. In the special case where  $\Xi$  is the whole space,

$\mathbb{R}^d$ , or some deterministic set  $D \subset \mathbb{R}^d$ ,  $\Gamma$  is a standard random field (with upper semi-continuous trajectories) on  $\mathbb{R}^d$  (respectively,  $D$ ).

We say that a RMCS,  $(\Xi, \Gamma)$ , is *stationary* if the random closed sets  $\tau(\Xi, \Gamma) + (x, 0)$  and  $\tau(\Xi, \Gamma)$  have the same distribution for all  $x \in \mathbb{R}^d$ . We say that  $(\Xi, \Gamma)$  is *isotropic* if  $\theta \circ \tau(\Xi, \Gamma)$  and  $\tau(\Xi, \Gamma)$  have the same distribution for all rotations  $\theta \in SO_{d+1}$  with  $\theta(\mathbb{R}^d \times \{0\}) = \mathbb{R}^d \times \{0\}$ . In the following, we assume that  $(\Xi, \Gamma)$  is a stationary RMCS such that  $\mathbb{P}(o \in \Xi) > 0$ , where  $o \in \mathbb{R}^d$  is the origin.

Let  $\Gamma'$  be an upper semi-continuous random field in  $\mathbb{R}^d$ . If  $\Xi$  and  $\Gamma'$  are independent and  $\Gamma = \Gamma'$  on  $\Xi$ , then  $(\Xi, \Gamma)$  is called a *random field model*. That is, a random field model is obtained by restricting a random field,  $\Gamma'$ , to a random domain,  $\Xi$ , that is independent of  $\Gamma'$ .

### 2.1. Second-order characteristics

The tests we consider in this paper are based on second-order characteristics of RMCSs. The first such characteristic is the mark-weighted  $K$ -function. This is an extension of the  $K$ -function, which is defined as follows. Let  $\Psi$  be the volume measure induced by  $\Xi$  (i.e.,  $\Psi(B) = |\Xi \cap B|$ ,  $B \in \mathcal{B}^d$ , where  $|\cdot|$  is the  $d$ -dimensional Lebesgue measure on the  $d$ -dimensional Borel  $\sigma$ -algebra  $\mathcal{B}^d$ ). Then,  $\mathbb{E}\Psi(B) = \lambda|B|$ , where  $\lambda = \mathbb{P}(o \in \Xi) > 0$  is the intensity of a stationary random measure  $\Psi$ . In general, the reduced second moment measure,  $\mathcal{K}$ , of a stationary random measure is defined through its Palm distribution; see [3, p. 33]. The  $K$ -function is given by  $K(r) = \mathcal{K}(b(o, r))$ , where  $b(o, r)$  is a ball of radius  $r > 0$  centered at  $o \in \mathbb{R}^d$ . In our setting, the  $K$ -function is of the form

$$K(r) = \frac{1}{\lambda} \mathbb{E}_o \Psi(b(o, r)), \quad r > 0,$$

where  $\mathbb{E}_o$  is the conditional expectation given  $o \in \Xi$ . Thus,  $\lambda K(r)$  is the mean volume of the set  $\Xi$  within a ball of radius  $r$  centered at a ‘typical’ point of  $\Xi$ . Using Fubini’s theorem, we get

$$K(r) = \frac{1}{\lambda^2} \int_{b(o, r)} C(x) dx, \tag{1}$$

where  $C(x) = \mathbb{P}(o \in \Xi, x \in \Xi)$  is the two-point coverage probability function of  $\Xi$ . Although the notion of a  $K$ -function has already been extended to random closed sets (see, e.g., [1] and [10]), it has not yet, to our knowledge,

been extended to RMCSs. We extend it as follows. We define  $\tilde{\Psi}$ , the mark-weighted version of  $\Psi$ , by

$$\tilde{\Psi}(B) = \int_B \Gamma(x) \Psi(dx), \quad B \in \mathcal{B}^d.$$

Here, we assume that  $\Gamma$  is non-negative and the integral is finite for any bounded Borel set  $B$ . Then  $\tilde{\Psi}$  is a stationary random measure. Its intensity,  $\tilde{\lambda}$ , is the mean of the integral of marks per unit volume. It satisfies  $\tilde{\lambda} = \lambda \mathbb{E}_o \Gamma(o)$  and we assume that  $0 < \tilde{\lambda} < \infty$ . Under these conditions, the  $K$ -function of  $\tilde{\Psi}$  is given by

$$\tilde{K}(r) = \frac{1}{\tilde{\lambda}} \tilde{\mathbb{E}}_o \tilde{\Psi}(b(o, r)), \quad r > 0, \quad (2)$$

where  $\tilde{\mathbb{E}}_o$  is the expectation with respect to the Palm distribution of  $\tilde{\Psi}$  at  $o$ . The quantity  $\tilde{\lambda} \tilde{K}(r)$  is the mean of the integral of marks within a ball of radius  $r$  centered at a ‘typical’ point of the mark-weighted version of  $\Xi$ . It means that the volume in the definition of  $K(r)$  is replaced by a ‘mark-weighted volume’. If  $\mathbb{E} \Gamma(o)^2 < \infty$ , the  $K$ -function of  $\Psi$  can be rewritten as

$$\tilde{K}(r) = \frac{1}{\tilde{\lambda}^2} \int_{b(o, r)} \tilde{C}(x) dx,$$

where  $\tilde{C}(x) = \mathbb{E}[\Gamma(o)\Gamma(x) \mathbb{I}\{o \in \Xi, x \in \Xi\}]$  and  $\mathbb{I}(A)$  denotes the indicator of the set  $A$ . If we put  $t(\gamma_1, \gamma_2) = \gamma_1 \gamma_2$ , then

$$\int_{b(o, r)} \tilde{C}(x) dx = \lambda \mathbb{E}_o \int_{b(o, r)} t(\Gamma(o), \Gamma(x)) \Psi(dx).$$

Motivated by this, and extending the approach proposed in [9, p. 351], we can define the general mark-weighted  $K$ -function for the RMCS  $(\Xi, \Gamma)$  by

$$K_t(r) = \frac{1}{\lambda c_t} \mathbb{E}_o \int_{b(o, r)} t(\Gamma(o), \Gamma(x)) \Psi(dx), \quad r > 0, \quad (3)$$

where  $c_t = \int \int t(\gamma_1, \gamma_2) \mathbb{Q}(d\gamma_1) \mathbb{Q}(d\gamma_2)$ ,  $t$  is a non-negative measurable test function which depends on two marks and  $\mathbb{Q}$  is the conditional distribution of  $\Gamma(o)$  given  $o \in \Xi$ . The denominator of  $K_t(r)$  is assumed to be positive and

finite. In particular, the test function  $t(\gamma_1, \gamma_2) = \gamma_1\gamma_2$  gives  $K_t(r) = \tilde{K}(r)$  defined in (2). The test function  $t(\gamma_1, \gamma_2) = \gamma_1$  in (3) yields

$$K_\Gamma(r) = \frac{\mathbb{E}_o[\Gamma(o)\Psi(b(o, r))]}{\lambda \mathbb{E}_o\Gamma(o)} = \frac{1}{\tilde{\lambda}} \mathbb{E}_o\tilde{\Psi}(b(o, r)) = \frac{1}{\lambda} \tilde{\mathbb{E}}_o\Psi(b(o, r)).$$

This formulation shows that  $\tilde{\lambda}K_\Gamma(r)$  can be interpreted as the mean mark-weighted volume of the set  $\Xi$  within a ball of radius  $r$  centered at a ‘typical’ point of  $\Xi$ . The mark-weighted  $K$ -function,  $K_t(r)$ , is a cumulative characteristic.

Another second-order characteristic we consider is the  $\kappa_t$ -function, introduced in [2]. This is a non-cumulative characteristics. Given that  $\mathbb{P}(o, x \in \Xi) > 0$  and the conditional expectation in (4) is finite, we define  $\kappa_t$  by

$$\kappa_t(x) = \mathbb{E}_{o,x} t(\Gamma(o), \Gamma(x)), \quad x \in \mathbb{R}^d, \quad (4)$$

where  $\mathbb{E}_{o,x}[\cdot] = \mathbb{E}[\cdot \mid o, x \in \Xi]$ . A normalized version of  $\kappa_t$  is

$$k_t(x) = \frac{\kappa_t(x)}{c_t}, \quad x \in \mathbb{R}^d. \quad (5)$$

If  $(\Xi, \Gamma)$  is also isotropic, then  $\kappa_t(x)$  depends only on  $\|x\|$ , where  $\|\cdot\|$  is the Euclidean norm, and, with slight abuse of notation, we write  $\kappa_t(r) = \kappa_t(x)$  and  $k_t(r) = k_t(x)$  for  $\|x\| = r$ . The cumulative and non-cumulative functions are related by the identity

$$\lambda^2 K_t(r) = \int_{b(o,r)} C(x) k_t(x) dx. \quad (6)$$

In the isotropic case we get  $\lambda^2 K_t'(r) = \sigma_d r^{d-1} C(r) k_t(r)$ , where  $\sigma_d$  is the surface of the unit sphere in  $\mathbb{R}^d$  and  $C(r) = C(x)$  for  $\|x\| = r$ . A similar formula for marked point processes can be found in [9, p. 352].

In particular, the test function  $t(\gamma_1, \gamma_2) = \gamma_1\gamma_2$  in (5) leads to the so-called  $k_{\text{mm}}$ -function,

$$k_{\text{mm}}(x) = \frac{\mathbb{E}_{o,x}[\Gamma(o)\Gamma(x)]}{(\mathbb{E}_o\Gamma(o))^2}, \quad x \in \mathbb{R}^d. \quad (7)$$

For  $t(\gamma_1, \gamma_2) = \gamma_1$ , the resulting non-cumulative function,  $\kappa_e(x)$ , defined as

$$\kappa_e(x) = \mathbb{E}_{o,x}\Gamma(o), \quad x \in \mathbb{R}^d, \quad (8)$$

is called the  $E$ -function. The  $E$ -function normalized by the mean mark value is given by

$$k_e(x) = \frac{\kappa_e(x)}{\mathbb{E}_o\Gamma(o)} = \frac{\mathbb{E}_{o,x}\Gamma(o)}{\mathbb{E}_o\Gamma(o)}, \quad x \in \mathbb{R}^d. \quad (9)$$

Note that, under the random field model assumption, we have  $K_\Gamma(r) = K(r)$  and  $\kappa_e(x) = \mathbb{E}_o\Gamma(o)$ . However, the following example shows that  $K_\Gamma(r) = K(r)$  does not necessarily imply that  $(\Xi, \Gamma)$  is a random field model. Let  $\Xi$  be a stationary random closed set with  $K$ -function  $K(r)$  and let  $\Gamma(x) = \mu + d(x, \partial\Xi)\varepsilon(x)$  for  $x \in \Xi$ , where  $\mu > 0$  is a positive constant,  $d(x, \partial\Xi)$  is the distance of  $x$  to the boundary of  $\Xi$ , and  $\{\varepsilon(x) : x \in \mathbb{R}^d\}$  is a continuous centred random field that is independent of  $\Xi$ . Then,  $\mathbb{E}_o\Gamma(o) = \mu$  and  $\mathbb{E}_o[\Gamma(o)\Psi(b(o, r))] = \mu\mathbb{E}_o\Psi(b(o, r)) = \mu\lambda K(r)$ . This gives  $K_\Gamma(r) = K(r)$ .

## 2.2. Estimators of the second-order characteristics

In general, we consider a single realization of  $(\Xi, \Gamma)$  within a bounded window  $W \subset \mathbb{R}^d$ . In this setting, we estimate the considered second-order characteristics as follows.

In order to estimate the mark-weighted  $K$ -function,  $K_\Gamma$ , we select  $N$  test points,  $\xi_1, \dots, \xi_N$ , in  $W$  independently of  $(\Xi, \Gamma)$ . A natural estimator of  $\lambda K_\Gamma(r)$  is given by

$$\widehat{\lambda K_\Gamma(r)} = \frac{\sum_{i=1}^N \Gamma(\xi_i) \mathbb{I}\{\xi_i \in \Xi\} \Psi(b(\xi_i, r))}{\sum_{i=1}^N \Gamma(\xi_i) \mathbb{I}\{\xi_i \in \Xi\}}. \quad (10)$$

This is a ratio-unbiased estimator because

$$\mathbb{E} \sum_{i=1}^N \Gamma(\xi_i) \mathbb{I}\{\xi_i \in \Xi\} \Psi(b(\xi_i, r)) = N \mathbb{E} [\Gamma(o) \mathbb{I}\{o \in \Xi\} \Psi(b(o, r))]$$

and  $\mathbb{E} \sum_{i=1}^N \Gamma(\xi_i) = N \mathbb{E} [\Gamma(o) \mathbb{I}\{o \in \Xi\}]$ . In order to use the estimator given in (10), we need to be able to determine  $\Psi(b(\xi_i, r))$ . However, this may not be possible if  $\xi_i$  is close to the boundary of  $W$ . In order to avoid the resulting edge effects, we use minus edge correction. That is, we only consider the test points  $\xi_i$  lying in an eroded window  $W \ominus b(o, r) = \{x \in W : b(x, r) \subset W\}$ . We obtain an estimator of  $K_\Gamma(r)$  by dividing the right-hand side of (10) by the natural intensity estimator,  $\hat{\lambda} = \Psi(W)/|W|$ . This gives

$$\widehat{K_\Gamma(r)} = \frac{1}{\hat{\lambda}} \frac{\sum_{i=1}^N \Gamma(\xi_i) \mathbb{I}\{\xi_i \in \Xi\} \Psi(b(\xi_i, r))}{\sum_{i=1}^N \Gamma(\xi_i) \mathbb{I}\{\xi_i \in \Xi\}}. \quad (11)$$

Note that an estimator of this form was considered in [20].

An estimator of the other second order characteristic that we consider,  $\kappa_t(r)$ , was proposed in [20]. Let  $U \subset W$  be a finite test set (for example, the points of a lattice or a point process). Then, define

$$\hat{\kappa}_t(r) = \frac{1}{\#N_U(r)} \sum_{(x,y) \in N_U(r)} t(\Gamma(x), \Gamma(y)),$$

for all  $r$  such that  $N_U(r) = \{(x, y) \in (\Xi \cap U)^2 : \|x - y\| = r\} \neq \emptyset$ . In order to obtain estimates of  $\kappa_t$  for all  $r > 0$ , we use the estimator

$$\hat{\kappa}_t(r) = \frac{\sum_{\xi_i, \xi_j \in \Xi \cap \Phi \cap W : \xi_i \neq \xi_j} t(\Gamma(\xi_i), \Gamma(\xi_j)) k_b(r - \|\xi_i - \xi_j\|)}{\sum_{\xi_i, \xi_j \in \Xi \cap \Phi \cap W : \xi_i \neq \xi_j} k_b(r - \|\xi_i - \xi_j\|)}, \quad r > 0, \quad (12)$$

where  $k_b(r) = k(r/b)/b$  is some kernel function in  $\mathbb{R}$  with bandwidth  $b > 0$  and  $\Phi = \{\xi_i\}$  is a stationary and isotropic point process in  $\mathbb{R}^d$  that is independent of  $(\Xi, \Gamma)$ . As a special case of (12), we get

$$\hat{\kappa}_e(r) = \frac{\sum_{\xi_i, \xi_j \in \Xi \cap \Phi \cap W : \xi_i \neq \xi_j} \Gamma(\xi_i) k_b(r - \|\xi_i - \xi_j\|)}{\sum_{\xi_i, \xi_j \in \Xi \cap \Phi \cap W : \xi_i \neq \xi_j} k_b(r - \|\xi_i - \xi_j\|)}, \quad r > 0. \quad (13)$$

### 3. Tests of the random field model hypothesis

Given data from a single realization of a RMCS,  $(\Xi, \Gamma)$ , observed within a bounded window  $W \subset \mathbb{R}^d$ , we wish to test if the random field hypothesis is satisfied. That is, we wish to test the null hypothesis,  $H_0$ , against the alternative,  $H_A$ , where

$$\begin{aligned} H_0 &: (\Xi, \Gamma) \text{ is a random field model,} \\ H_A &: (\Xi, \Gamma) \text{ is not a random field model.} \end{aligned}$$

We develop two distinct tests, based on two different second-order characteristics of the RMCS. The first test is a *global rank envelope test* that considers the mark-weighted  $K$ -function,  $K_\Gamma$ . The second test uses a *subsampling* approach and considers the  $E$ -function,  $\kappa_e$ . Note that the tests do not test the above hypothesis in its entirety, but rather test that a second-order condition, which is necessary for the random field hypothesis to hold, is satisfied. Both tests make minimal assumptions about the underlying models from which the random field and random closed set come. As a result, they are generally

applicable and can be used when it is not *a priori* clear if the marks can be treated as a realization from a given random field model. In applications where additional information is available (for example, it is known that the marks come from a Gaussian random field model), it may be possible to develop more powerful tests that take this information into account.

### 3.1. Global rank envelope test

The mark-weighted  $K$ -function,  $K_\Gamma$ , was used in [16] to test the random labeling hypothesis for marked point processes. We extend this approach to RMCSs. In this setting, it is necessary to choose an appropriate set of test points for estimating  $K_\Gamma$ . As will be seen, the choice of test point pattern is critical to the success of the test.

#### 3.1.1. The test

Recall that, under the null hypothesis, the mark-weighted  $K$ -function is the same as the non-weighted  $K$ -function. That is,  $K_\Gamma = K$ . We can test whether this is the case or not using a global rank envelope test.

The basic idea, developed in [17], is the following. Suppose we calculate the values of a test characteristic,  $T_0(r)$ , at  $\ell$  points,  $r_1, \dots, r_\ell$ . We take this, as the test characteristic corresponding to the data. Furthermore, suppose it is possible to generate  $q$  replicates,  $T_1(r), \dots, T_q(r)$ , of this test characteristic under the null hypothesis. We can then conduct a test of the null hypothesis by comparing these replicates with  $T_0(r)$ . This is done by ranking  $T_0, \dots, T_q$  based on how extreme their values are at  $r_1, \dots, r_\ell$ . More precisely, for each  $r \in \{r_1, \dots, r_\ell\}$ , we order the values of the test characteristics as  $T_{(0)}(r) \leq T_{(1)}(r) \leq \dots \leq T_{(q)}(r)$ . We then assign a pointwise rank of 1 to the characteristics with the largest and smallest values, a pointwise rank of 2 to the characteristics with the second smallest and second largest values, and so on. More formally, we set  $R_{(0)}(r) = 1$ ,  $R_{(q)}(r) = 1$ ,  $R_{(1)}(r) = 2$ ,  $R_{(q-1)}(r) = 2$ , etc. If there are ties in the values  $T_i(r)$ , we use the mean of the corresponding ranks. For example, if  $T_{(0)}(r) = T_{(1)}(r) < T_{(2)}(r)$ , then  $R_{(0)}(r) = R_{(1)}(r) = 1.5$ . The global rank of a characteristic,  $T_i$ , is then given by its lowest pointwise rank, i.e.,  $R_i = \min\{R_i(r), r \in \{r_1, \dots, r_\ell\}\}$ . Using these ranks, we can estimate the probability that the characteristic  $T_0(r)$  is observed under the null hypothesis. A consistent interval containing the  $p$ -value can be estimated by  $(p_{\text{low}}, p_{\text{upp}})$ , where

$$p_{\text{low}} = 1 - \frac{1}{q+1} \sum_{i=1}^q \mathbb{I}\{R_i \geq R_0\}, \quad p_{\text{upp}} = 1 - \frac{1}{q+1} \sum_{i=1}^q \mathbb{I}\{R_i > R_0\}.$$

In this paper, we reject  $H_0$  if  $(p_{\text{upp}} + p_{\text{low}})/2 < \alpha$ , where  $\alpha$  is a prescribed significance level. However, a more conservative approach can be taken by choosing  $p_{\text{upp}}$  as the  $p$ -value.

In our setting, the characteristic of interest is an estimate of  $K_\Gamma$ , the mark-weighted  $K$ -function. As described in Section 2.2, this function is estimated using a set of test points. In order to apply the envelope test, we need to be able to generate replicates of the test characteristic under the null hypothesis. This can be done using random reallocation of marks; see [9, Section 7.5] for the particular case of the test of independent marking for marked point processes. That is, we generate estimates of the test characteristic by keeping the spatial locations of the test points used to estimate  $K_\Gamma$  from the observed data but generating random permutations of the marks. In order for random reallocation to work, the resulting test characteristics must be exchangeable (i.e., permutation invariant) under the null hypothesis; see [17]. The exchangeability criterion is satisfied if we impose a somewhat stronger condition that the marks are independent of one another. In order for this to be the case, we require that, conditional on  $\Xi$ , the random field,  $\Gamma$ , is  $m$ -dependent (see [4]) for some  $m \geq 0$  and the minimal distance between test points is at least  $m$ .

Given a prescribed level of significance,  $\alpha$ , our test procedure is as follows.

1. Select test points: choose  $N$  test points,  $\xi_1, \dots, \xi_N \in W$ , independently of  $(\Xi, \Gamma)$ , such that  $\|\xi_i - \xi_j\| > m$  for all  $i \neq j$  and let  $\mathcal{I} = \{i : \xi_i \in \Xi\}$ .
2. Estimate: estimate  $K_\Gamma$  by  $\widehat{K}_{\Gamma,0}$  using the estimator given in (11).
3. Generate random reallocations: generate  $q$  random permutations of  $\{\Gamma(\xi_i) : i \in \mathcal{I}\}$  and estimate  $K_\Gamma$  for each permutation, denoting the estimates  $\widehat{K}_{\Gamma,1}, \dots, \widehat{K}_{\Gamma,q}$ .
4. Rank: for each  $r \in \{r_1, \dots, r_\ell\}$ , assign ranks to  $\widehat{K}_{\Gamma,0}, \dots, \widehat{K}_{\Gamma,q}$  as above.
6. Calculate  $p$ -values: estimate  $p_{\text{low}}$  and  $p_{\text{upp}}$  as above.
7. Decision: if  $(p_{\text{upp}} + p_{\text{low}})/2 < \alpha$ , reject  $H_0$ .

### 3.1.2. Choosing the test points

As discussed above, in order for our approach to work, it is necessary that the random field,  $\Gamma$ , is  $m$ -dependent given  $\Xi$  and that the test points are then chosen so that the minimal distance between any two points is  $m$ .

In practice,  $m$  is usually unknown and must be estimated. When  $(\Xi, \Gamma)$  is isotropic, we suggest using the  $k_{\text{mm}}$ -function defined in (7), which is a normalized special case of the  $\kappa_t$  function described above and can be estimated accordingly. We consider  $k_{\text{mm}}(r)$ , the isotropic form of  $k_{\text{mm}}(x)$ . This function takes a value of 1 at distances such that the marks are no longer correlated. Thus, we can choose  $m$  to be the value of  $r$  such that  $k_{\text{mm}}(r)$  appears to have converged to 1. Note that, in practice, it does not appear to matter too much if  $m$  is slightly underestimated.

Having decided on an appropriate minimum distance between points, we then wish to choose a point pattern that satisfies the following criteria:

1. the point pattern is independent of  $(\Xi, \Gamma)$ ,
2. the minimal distance between any two points is  $m$ ,
3. there are as many points in  $W$  as possible.

One possible choice for generating the test points is a hard-core process with hard-core distance  $m$ . One such process is the Matérn type II hard-core process, which is defined as follows. Let  $\Phi$  be a stationary Poisson point process,  $\{U(\xi), \xi \in \Phi\}$  be a sequence of i.i.d. uniform  $[0, 1]$  random variables which are independent of  $\Phi$ , and  $h > 0$  be a hard-core distance. Then, the Matérn type II hard-core process is defined as

$$\Phi_H = \{\xi \in \Phi : U(\xi) \leq U(\nu) \text{ for all } \nu \in \Phi \text{ such that } \|\xi - \nu\| < h\}.$$

However, although this process satisfies the first two criteria, it does not maximize the number of points in  $W$ .

A better choice is to use the mid points of an optimal packing of spheres with radius  $m/2$ , for example, a hexagonal close packing. In practice, we construct an optimal packing in a window,  $W_2$ , such that  $W \subset W_2$ . We then place  $W$  uniformly at random in  $W_2$  and take the midpoints contained in  $W$  as the test point pattern. As will be seen in Section 4, this choice of test point pattern appears to be optimal.

### 3.2. *Subsampling test*

The second test we consider is based on the  $E$ -function, defined in (8). This asymptotic test requires the additional assumption that  $(\Xi, \Gamma)$  is isotropic. In order to calculate the test statistics, it uses subsampling to estimate an asymptotic covariance matrix. The size of the subsampling window must be chosen carefully.

Under the null hypothesis, the function  $k_e(x)$  given in (9) is a constant function equal to 1 for all vectors  $x$ . Thus, if the null hypothesis holds, the estimator (13) should be close to a constant function. This will be true if the random variables  $\{\Gamma(\xi_i)\}$  are independent of the  $\{\xi_i\}$ . Defining the marked point process  $\tilde{\Phi} = \{(\xi_i, \Gamma(\xi_i)) : \xi_i \in \Xi\}$ , this requirement is then equivalent to the requirement that  $\tilde{\Phi}$  satisfies the random field model hypothesis for marked point processes. Therefore, we can test the random field model hypothesis for  $(\Xi, \Gamma)$  by testing for the independence between the marks and points of  $\tilde{\Phi}$ .

### 3.2.1. The test

Note that the  $E$ -function estimate obtained using (13) is also an estimate of the  $E$ -function of  $\tilde{\Phi}$ . Thus, we can apply a test of the random field model hypothesis for marked point processes that is based on the  $E$ -function. Two such tests are described in [8] and [19]. We adopt the approach in [8], which is as follows. By considering a set of lags,  $\{r_1, \dots, r_\ell\}$ , we obtain a vector of pointwise estimates,  $\mathbf{K} = (\hat{\kappa}_e(r_1), \dots, \hat{\kappa}_e(r_\ell))$ . It can be shown that, under certain regularity conditions given in [8], the standardized version of  $\mathbf{K}$  is asymptotically normal (as  $W$  increases without bound) with asymptotic covariance matrix  $\Sigma$ . Define the  $(\ell - 1) \times \ell$  matrix  $\mathbf{A} = (a_{ij})$ , where  $a_{i1} = 1$  and  $a_{i,i+1} = -1$  for  $i = 1, \dots, \ell - 1$  and  $a_{ij} = 0$  otherwise. Then, we can test for independence between the marks and points by testing the hypothesis  $\mathbf{A}\mathbf{E}\mathbf{K} = 0$ . Consider the test statistic

$$T = b|W|(\mathbf{A}\mathbf{K})'(\mathbf{A}\hat{\Sigma}\mathbf{A}')^{-1}(\mathbf{A}\mathbf{K}), \quad (14)$$

where  $b$  is the bandwidth of the kernel  $k_b$  and  $\hat{\Sigma}$  is a consistent estimator of  $\Sigma$  obtained by subsampling. This statistic is asymptotically  $\chi^2$  distributed with  $\ell - 1$  degrees of freedom. The subsampling is carried out by considering a subsampling window,  $W_0$ , which is a rescaled version of  $W$ . This window must be smaller than  $W$  but large enough that  $\hat{\kappa}_e(r)$  can be estimated for all  $r \in \{r_1, \dots, r_\ell\}$ . Then,  $\hat{\Sigma}$  is estimated from the empirical covariances of the estimates  $\hat{\kappa}_e(r)$ ,  $r \in \{r_1, \dots, r_\ell\}$ , that are calculated from the points  $\tilde{\Phi} \cap (y + W_0) \subset W$ , where  $y \in \{x \in W : x + W_0 \subset W\}$ ; see [8] for details. In practice, we only consider a finite number of values of  $y$ . Thus, for a given level of significance  $\alpha$ , and a given subsampling window  $W_0$ , the test procedure is as follows.

1. Select test points: generate an isotropic and stationary point process,  $\Phi$ . Assign the corresponding marks to obtain  $\tilde{\Phi}$ .
2. Estimate: using  $\tilde{\Phi}$ , estimate  $\hat{\Sigma}$  via the subsampling approach described above.
3. Calculate test statistic: calculate  $T$ , given in (14).
4. Decision: reject  $H_0$  if  $T > \chi_{\ell-1, 1-\alpha}^2$ , where  $\chi_{\ell-1, 1-\alpha}^2$  is the  $(1 - \alpha)$  quantile of the  $\chi^2$  distribution with  $\ell - 1$  degrees of freedom.

### 3.2.2. Choice of test points

Unlike the envelope test, there is no minimal distance restriction when choosing the test points for the subsampling test. Here, the only restriction is that the points are from a realization of a stationary and isotropic point process that is independent of  $(\Xi, \Gamma)$ . As we wish to maximize the number of points in  $\Xi \cap \tilde{\Phi}$ , we use a low discrepancy sequence for the test points. This is a sequence of points that is designed to cover a space as uniformly as possible, typically filling the space more effectively than lattices (such as hexagonal packings); see [14]. Although such sequences are deterministic, they can be randomly shifted and rotated, resulting in a stationary and isotropic point process.

In this paper, we use a Halton sequence for the test points. This is based on base- $b$  representations of the integers, where  $b > 0$  is an arbitrary integer. Observe that any integer,  $k$ , can be written as  $k = \sum_{i=1}^r a_i b^{i-1}$  for some finite  $r$  and  $a_1, \dots, a_r \in \{0, \dots, b-1\}$ . The radical inverse of  $k$  is then given by  $\sum_{i=1}^r a_i b^{-i}$ . Let  $\{u_k^1\}, \dots, \{u_k^d\}$  be radical inverses of the integers  $k = 1, 2, \dots$ , in relatively prime bases  $b_1, \dots, b_d$ . The sequence  $\{(u_k^1, \dots, u_k^d)\}_{k=1}^\infty$  then forms a Halton sequence in  $[0, 1]^d$ . This can be easily transformed into a sequence in a bounded rectangular window  $W \subset \mathbb{R}^d$ . For more details on such sequences; see [14]. An example of a Halton sequence in the planar rectangular window is given in Figure 1.

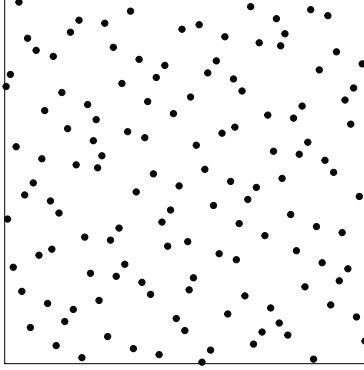


Figure 1: Halton sequence of 133 points in a square window.

#### 4. Simulation study

In this section, we carry out simulation studies of the two tests described above in order to investigate their power and general performance. We consider two different random closed set models in  $\mathbb{R}^2$ : a marked Boolean model and an excursion set model. In order to study how the rejection rates of the tests change as a function of the degree of dependence between the random field and the random closed set, we consider marks of the form

$$\Gamma(x) = (1 - \beta)\Gamma_1(x) + \beta\Gamma_2(x), \quad x \in \mathbb{R}^2, \quad \beta \in [0, 1],$$

where  $\Gamma_1$  is a random field independent of  $\Xi$ ,  $\Gamma_2$  is a function of  $\Xi$ , and the parameter  $\beta$  controls the degree of dependence between  $\Xi$  and  $\Gamma$ . The models for  $\Gamma_1$  and  $\Gamma_2$  will be specified in Sections 4.1 and 4.2. In both cases the observation window will be  $W = [0, 1500]^2$  and the range of dependence will be  $m = 140$ .

In the case of the first test, we consider three different choices of test point pattern: hexagonal close packings, the Matérn type II hard-core process, and the Poisson process. Typical examples of these point patterns are illustrated in Figure 2. By considering different point patterns, we are able to explore how the choice of test points influences the power and reliability of the envelope test. The test is always based on  $q = 4999$  permutations and the test statistics are evaluated at  $\ell = 15$  lags,  $r_i = 5i$ ,  $i = 1, \dots, 15$ . This range of lags was chosen because the estimates of the mark-weighted  $K$ -function become less accurate for larger values of  $r$ .

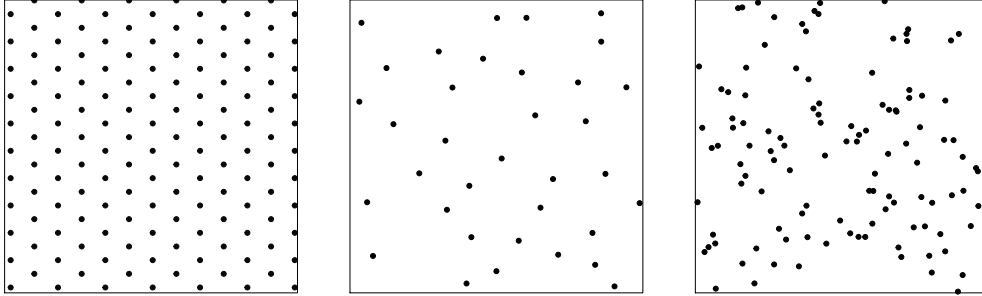


Figure 2: Left: a hexagonal configuration with minimal distance 140; middle: a Matérn type II hard-core point process with hard-core distance 140; right: a Poisson point process.

For the second test, we consider two different subsampling windows:  $W_0 = [0, 400]^2$  and  $W_0 = [0, 600]^2$ . We use marked points obtained from the intersection of a Halton sequence of 10 000 points in  $W$  with the random closed set (where the marks are the values of  $\Gamma$  at the location of the points). The test statistics are evaluated at  $\ell = 15$  lags  $r_i = 5i$ ,  $i = 1, \dots, 15$ .

The experiments are carried out as follows. For each random closed set model, we simulate  $n_s = 100$  realizations of the random closed set and the independent random field  $\Gamma_1$ . As  $\Gamma_2$  is a deterministic function of  $\Xi$ , this does not need to be simulated. The same realizations of  $\Xi, \Gamma_1$  and  $\Gamma_2$  are used for each value of  $\beta$  we consider. For each realization of the random closed set,  $\Xi$ , we generate  $n_p = 10$  realizations of each test point pattern. These realizations are also saved and used for each value of  $\beta$ . Thus, for each value of  $\beta$ , we carry out  $n_s \cdot n_p = 1000$  tests. These tests are performed at a fixed significance level of  $\alpha = 0.05$ . The rejection rates we obtain are simply the percentage of tests that are rejected.

#### 4.1. Marked Boolean model

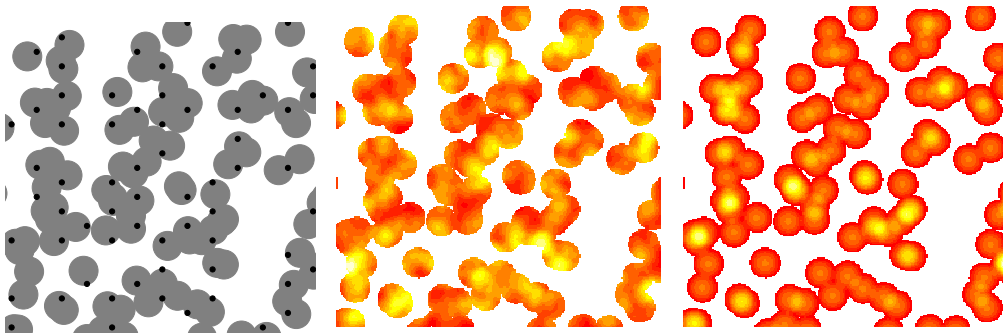


Figure 3: Left: A realization of the Boolean model overlaid with test points obtained from a hexagonal close packing with minimal distance 140. Middle: A realization of the independent mark field,  $\Gamma_1$ . Right: A realization of the dependent mark field,  $\Gamma_2$ .

One of the simplest random closed set models is a Boolean model of balls in  $\mathbb{R}^2$ ,

$$\Xi = \bigcup_{i \in \mathbb{N}} (\xi_i + z),$$

where  $z = b(o, r_0)$  for some  $r_0 > 0$  and the points,  $\{\xi_i\}$ , form a stationary Poisson point process,  $\Phi$ , in  $\mathbb{R}^2$  with some intensity  $\lambda_\Phi$ . For the marking field,  $\Gamma_2$ , we use

$$\Gamma_2(x) = c_{\Gamma_2} \sum_{\xi_i \in \Phi} k(\|x - \xi_i\|), \quad x \in \mathbb{R}^2, \quad (15)$$

where

$$k(r) = \max \left\{ 1 - \left( \frac{r}{r_0} \right)^2, 0 \right\}, \quad r \geq 0,$$

and  $c_{\Gamma_2} \in \mathbb{R}$  is a scaling constant. We use a shot-noise Poisson random field, independent of  $\Xi$ , for the independent marking field,  $\Gamma_1$ . That is, we take

$$\Gamma_1(x) = c_{\Gamma_1} \sum_{\xi_i \in \Phi_\Gamma} k(\|x - \xi_i\|), \quad x \in \mathbb{R}^2,$$

where  $\Phi_\Gamma$  is a stationary Poisson point process in  $\mathbb{R}^2$  with some intensity  $\lambda_\Gamma$  which is independent of  $\Phi$ ,  $k$  is defined as above and  $c_{\Gamma_1} \in \mathbb{R}$  is a scaling constant.

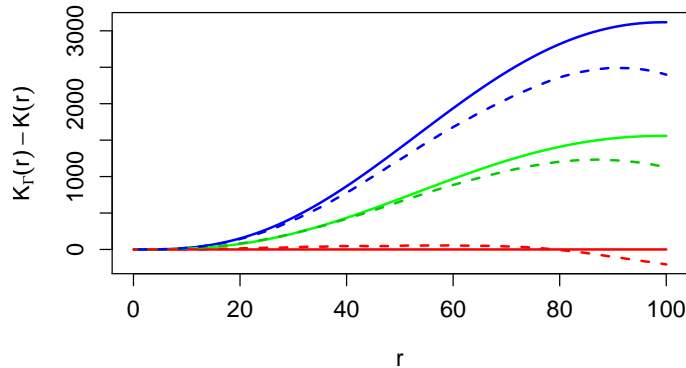


Figure 4: Theoretical values (full lines) of  $K_{\Gamma}(r) - K(r)$  for the marked Boolean model with three different  $\beta$ , degrees of dependence between  $\Xi$  and  $\Gamma$ . For comparison the estimated functions (dashed lines) based on data and test points from Figure 3 are shown. Red:  $\beta = 0$ ; green:  $\beta = 0.5$ ; blue:  $\beta = 1$ .

The intensity of volume measure induced by the Boolean model  $\Xi$  is equal to its volume fraction and is given by  $\lambda = 1 - \exp\{-\lambda_{\Phi}\pi r_0^2\}$ ; see [5, (3.15)]. The two-point probability function of  $\Xi$  is  $C(x) = 2\lambda - 1 + (1 - \lambda)^2 \exp\{\lambda_{\Phi}|z \cap (z + x)|\}$ ; see [5, (3.18)]. Exploiting these formulas and (1), we obtain the  $K$ -function of the volume measure induced by  $\Xi$ ,

$$K(r) = \pi r^2 + 2\pi \frac{(1 - \lambda)^2}{\lambda^2} \int_0^r s (e^{\lambda_{\Phi}\gamma(s)} - 1) ds, \quad (16)$$

where  $\gamma(s) = |z \cap (z + su)|$  for arbitrary  $u$  with  $\|u\| = 1$ .

The mark-weighted  $K$ -function of the RMCS  $(\Xi, \Gamma_2)$  may be expressed by applying the Slivnyak-Mecke formula; see [5, (4.71)]. We get

$$K_{\Gamma_2}(r) = \pi r^2 + \frac{4(1 - \lambda)}{\lambda r_0^2} \int_0^r s q(s) ds, \quad (17)$$

where  $q(\|y\|) = \int_{b(o, r_0) \cap b(y, r_0)} k(x) dx$ . The mark-weighted  $K$ -function of the RMCS  $(\Xi, \Gamma)$  then becomes

$$K_{\Gamma}(r) = \frac{(1 - \beta)\mathbb{E}\Gamma_1(o)K(r) + \beta\mathbb{E}_o\Gamma_2(o)K_{\Gamma_2}(r)}{(1 - \beta)\mathbb{E}\Gamma_1(o) + \beta\mathbb{E}_o\Gamma_2(o)}, \quad (18)$$

where  $\mathbb{E}\Gamma_1(o) = c_{\Gamma_1}\lambda_{\Gamma}\pi r_0^2/2$  and  $\mathbb{E}_o\Gamma_2(o) = c_{\Gamma_2}\lambda_{\Phi}\pi r_0^2/2\lambda$  can be obtained from Slivnyak-Mecke formula.

Since our model is isotropic, the normalized  $E$ -function,  $k_e$ , is given by

$$k_e(r) = \frac{\lambda^2 K'_{\Gamma}(r)}{2\pi r C(r)}, \quad r > 0. \quad (19)$$

This relation follows directly from (6).

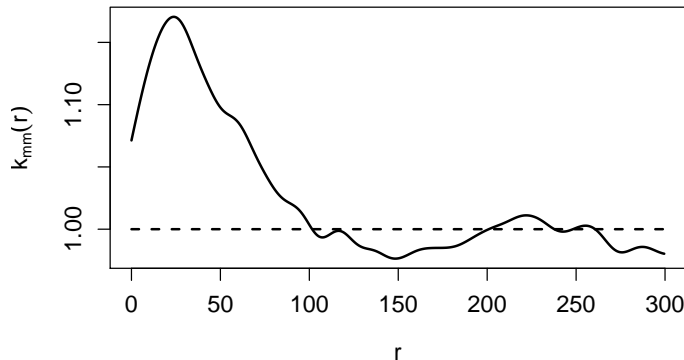


Figure 5: An estimate of the  $k_{\text{mm}}$ -function for the marked Boolean model with  $\beta = 0$ .

For our experiments, we consider a 2-dimensional Boolean model in an observation window,  $W = [0, 1500]^2 \subset \mathbb{R}^2$ . We take  $r_0 = 70$ ,  $\lambda_{\Phi} = 100/|W|$ ,  $\lambda_{\Gamma} = 1000/|W|$ ,  $c_{\Gamma_2} = 13$ . The parameter  $c_{\Gamma_1} = 2.624$  is chosen so that  $\mathbb{E}\Gamma_1(o) = \mathbb{E}_o\Gamma_2(o)$ . Hence, by (18),  $K_{\Gamma}$  is a convex combination of  $K(r)$  and  $K_{\Gamma_2}(r)$ . A simulated realization of  $\Xi$  in  $W$  is shown in Figure 3, together with a hexagonal close packing sequence of test points with minimal distance equal to 140. Figure 3 also shows realizations of the mark fields  $\Gamma_1$  and  $\Gamma_2$ .

Figure 4 shows the mark-weighted  $K$ -functions, computed from (16), (17) and (18), for three different values of  $\beta$ . For better visualization we subtracted  $K(r)$ . Our envelope test is based on the estimates of this characteristics. Figure 4 shows estimates for given realizations of  $\Gamma_1$  and  $\Gamma_2$  (which are illustrated in Figure 3). Under the null hypothesis,  $K_{\Gamma} = K$  (red curve,  $\beta = 0$ ). For larger values of  $\beta$  the deviation of  $K_{\Gamma}(r)$  from  $K(r)$  increases and therefore the null hypothesis is more likely to be rejected.

The theoretical range of dependence for  $\Gamma$  is  $m = 2r_0 = 140$ . In practice, as discussed in Section 3.1.2, this is usually unknown and must be estimated. Figure 5 shows an estimate of the  $k_{\text{mm}}$ -function based on one realization of the model with  $\beta = 0$  (shown in Figure 3). This yields a rough estimate of  $\hat{m} \in [100, 120]$ .

In our experiments, we consider two different hexagonal close packings: one with minimal distance 140 (which, in the best case, results in 133 points in  $W$ ) and one with minimal distance 267 (best case, 37 points in  $W$ ). We also consider a Poisson process with intensity  $133/|W|$  (on average 133 points in  $W$ ) and a Matérn type II hard-core point process with intensity  $300/|W|$  and minimal distance 140 (on average 37 points in  $W$ ). The second hexagonal packing is considered because it has the same intensity as the Matérn process. Note that the hexagonal packings and the Matérn hard-core process satisfy the minimal distance requirement for the envelope test.

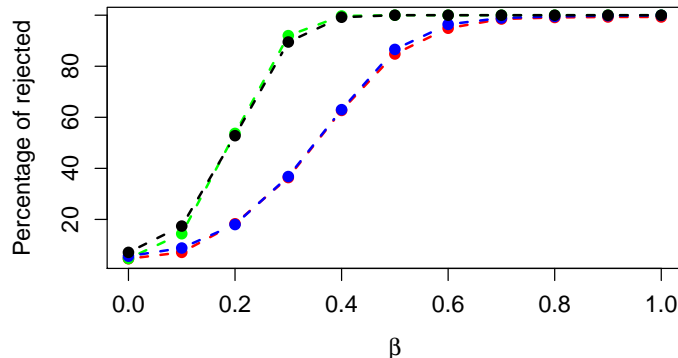


Figure 6: Rejection rates of the envelope test applied to the marked Boolean model using four different choices of test point pattern. Green: hexagonal packing with minimum distance 140; black: Poisson process; red: Matérn type II hard-core process; blue: hexagonal packing with minimum distance 267.

Figure 6 shows how the four different test point patterns perform as  $\beta$  varies. As expected, the two test point patterns with the most points have significantly higher powers. They both achieve powers close to 1 for  $\beta \geq 0.4$ . The two point patterns with less points (the Matérn hard-core process and the hexagonal packing with minimum distance 267) have significantly

lower power. Furthermore, as expected, the Poisson process, which does not guarantee a minimal distance between points, does not have the desired type I error (with 0.071 being significantly larger than 0.05). Thus, the hexagonal packing with minimal distance 140 (which maximizes the number of test points while maintaining the desired minimum distance) is clearly the optimal choice of test point pattern.

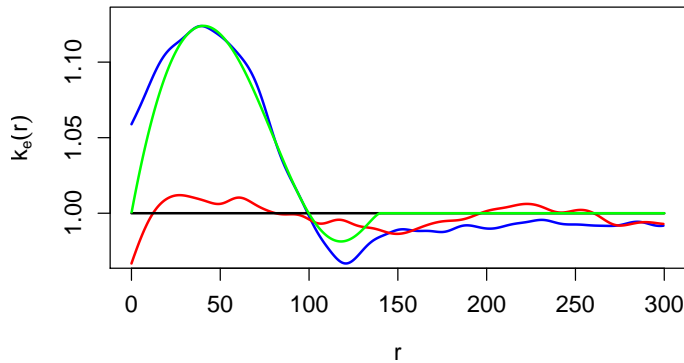


Figure 7: Estimates of the  $E$ -function,  $k_e$ , for marked Boolean models. Blue:  $\beta = 1$ ; red:  $\beta = 0$ . The theoretical value of  $k_e$  under  $H_0$  is represented by the horizontal line. The theoretical value of  $k_e$  for  $\beta = 1$  is shown by the green line.

Recall that the second test is based on the  $E$ -function,  $\kappa_e$ . The normalized version,  $k_e$ , is given by (19). Figure 7 shows the theoretical values of  $k_e$  under the null hypothesis ( $\beta = 0$ ) and for  $\beta = 1$ , together with estimates of  $k_e$  obtained from realizations of the RMCS with  $\beta = 0$  and  $\beta = 1$  (Figure 3). Based on a visual examination, one would reject the null hypothesis for the  $\beta = 1$  case, as the function is clearly not constant.

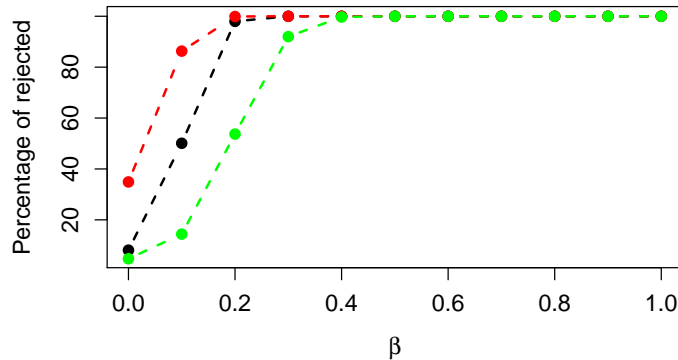


Figure 8: Rejection rates of the subsampling test applied to the marked Boolean model. Red:  $W_0 = [0, 600]^2$ ; black:  $W_0 = [0, 400]^2$ . For comparison, the rejection rates of the envelope test using the hexagonal packing with minimal distance 140 are shown in green.

Figure 8 illustrates the performance of the subsampling tests for both choices of subsampling window,  $W_0$ . For comparison, the envelope test using the hexagonal close packing with 140 points is included. It is immediately apparent from the results that the performance of the subsampling test depends strongly on the choice of subsampling window. The test with the subsampling window of size  $400 \times 400$  has a higher power than the envelope test while approximately maintaining the desired type I error. In contrast, the test with the subsampling window of size  $600 \times 600$  has a much higher type I error than desired.

#### 4.2. Excursion set model

The second random closed set model we consider is the excursion set of a Gaussian random field,  $\Gamma'$ . Here, the random closed set,  $\Xi$ , is given by

$$\Xi = \{x \in \mathbb{R}^2 : \Gamma'(x) \geq u\},$$

where  $u \in \mathbb{R}$  is a fixed threshold. We take the marking field,  $\Gamma_2$ , to be  $\Gamma'$  restricted to  $\Xi$ . In this example, we take  $u = 1$  to ensure that the marks are positive. The marking field,  $\Gamma_1$ , is taken to be another Gaussian random field, independent of  $\Gamma'$ , that is again restricted to  $\Xi$ . We take the absolute value of this field in order to obtain positive marks.

Both Gaussian random fields are simulated in the window  $W = [0, 1500]^2$ . Their expectation is taken to be 1 and we consider a circular covariance function

$$C_{\Gamma}(r) = 1 - \frac{2}{\pi} \left( r\sqrt{R^2 - r^2}/R^2 + \arcsin(r/R) \right) \mathbb{I}\{0 \leq r \leq R\},$$

where  $R = 140$ . A realization of the excursion set, together with test points obtained using a hexagonal close packing, is shown in Figure 9.

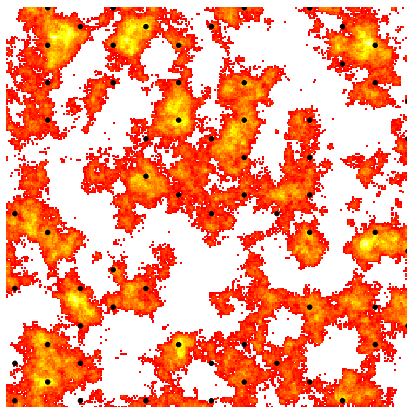


Figure 9: A realization of the excursion set model overlaid by a hexagonal sequence of test points with minimal distance 140.

The theoretical range of dependence for  $\Gamma$  is  $m = R = 140$ . We use the same test points as for a marked Boolean model, i.e. two hexagonal packings, with minimal distances 140 and 267, a Poisson process with intensity  $133/|W|$  and a Matérn type II hard-core process with intensity  $300/|W|$  and hard-core radius 140.

Figure 10 shows the performance of the global rank envelope test for different choices of test point patterns. As with the marked Boolean model, the patterns with more points (the Poisson process and the hexagonal packing with minimal distance 140) have much higher power than the tests with less points. Again, the Poisson point patterns (which do not have a minimal distance between points) result in a much higher type I error than desired (here, 0.078 compared to 0.045 for the hexagonal packing with minimal distance 140).

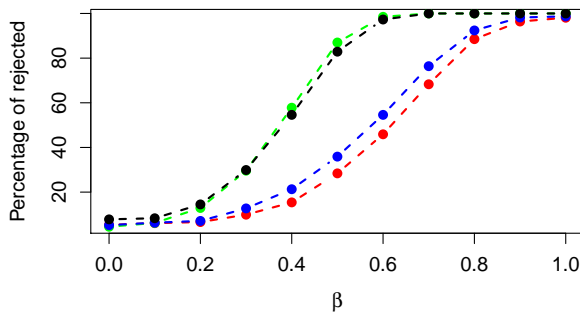


Figure 10: Rejection rates of the global rank envelope test applied to the excursion set model. Green: hexagonal packing with minimal distance 140; black: Poisson process; red: Matérn type II hard-core process; blue: hexagonal packing with minimal distance 267.

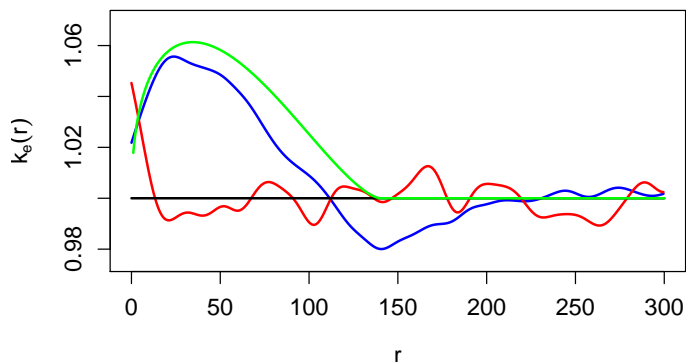


Figure 11: Estimates of the  $E$ -function,  $k_e$ , for the excursion set model. Blue:  $\beta = 1$ ; red:  $\beta = 0$ . The theoretical value of  $k_e$  under  $H_0$  is represented by the horizontal line. The theoretical value for  $\beta = 1$  is shown by the green line.

The  $E$ -function for  $\beta = 1$  has the form

$$\kappa_e(r) = u + \sqrt{\frac{\pi}{2}} \frac{1 + C_\Gamma(r)}{\arcsin C_\Gamma(r) + \pi/2};$$

see [2, Theorem 2]. The normalized  $E$ -function,  $k_e$ , is obtained by dividing by  $\mathbb{E}_o\Gamma(o) = 1 + \sqrt{2/\pi}$ . Figure 11 shows the theoretical value of  $k_e$  under

the null hypothesis ( $\beta = 0$ ) and for  $\beta = 1$ , together with estimates of  $k_e$  obtained from realizations of the RMCS with  $\beta = 0$  and  $\beta = 1$ . Based on a visual examination, one would reject the null hypothesis for the  $\beta = 1$  case, as the function is clearly not constant. In the  $\beta = 0$  case, the outcome is not so clear.

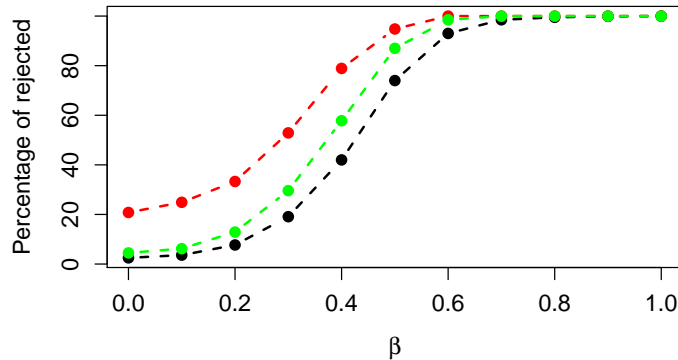


Figure 12: Rejection rates of the subsampling test applied to the excursion set model. Red:  $W_0 = [0, 600]^2$ ; black:  $W_0 = [0, 400]^2$ . For comparison, the rejection rates of the global rank envelope test using a hexagonal packing with minimal distance 140 are shown in green.

The results obtained from the subsampling tests are shown in Figure 12. The results of the global rank envelope test using a hexagonal close packing with minimal distance 140 are included for comparison. As in the marked Boolean model case, the test using a subsampling window of size  $600 \times 600$  results in a very incorrect type I error (0.208 compared to 0.045 for the envelope test). Here, the subsampling window of size  $400 \times 400$  also seems to result in an incorrect type I error (0.025). In addition, the power of the tests when using this subsampling window is lower than the power of the global rank envelope test. The performance of the subsampling tests also depends on the choice of the bandwidth,  $b$ , in the kernel estimator of  $\kappa_e$ .

#### 4.3. Further discussion

In the scenarios considered above, the global rank envelope test with an enforced minimal distance between points appears to be more reliable than

the subsampling test. In particular, the global rank envelope test appears to perform very well when the test point pattern is a hexagonal close packing with minimal distance close to  $m$ , the range of dependency of the random field.

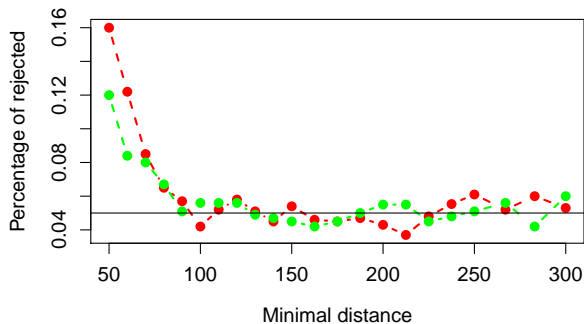


Figure 13: Rejection rates for the global rank envelope test with hexagonal close packing for models with  $\beta = 0$  (i.e., where the random field model hypothesis is satisfied). Green: marked Boolean model; red: excursion set model. The desired level of significance is shown by the horizontal line.

In order to demonstrate that the envelope test is quite robust with respect to incorrect estimates of  $m$ , we carried out experiments where we estimated the type I error of the envelope test using hexagonal close packings with different minimum distances. We considered the models above with  $\beta = 0$ . The results are illustrated in Figure 13. For both models, the theoretical value of  $m$  is 140. However, the desired type I error is achieved for lower minimum distances. Note, however, that these results show that the minimum distance between points should not be too small, as this results in a loss of control over the type I error. This argues against the use of a Poisson process as a test point pattern.

## 5. Data examples

In this section, we apply our testing methodology to both macroscopic and microscopic real world data. We first consider an application to radar data on precipitation in Germany. We also apply our methodology to transmission electron microscopy (TEM) data that describe the nanostructure of an organic semiconductor.

### 5.1. Radar data

In [13], a stochastic model is introduced that describes precipitation over Germany. It models both the occurrence of precipitation cells and the amount of precipitation at the locations where precipitation occurs. Thus, precipitation can be described by a RMCS.

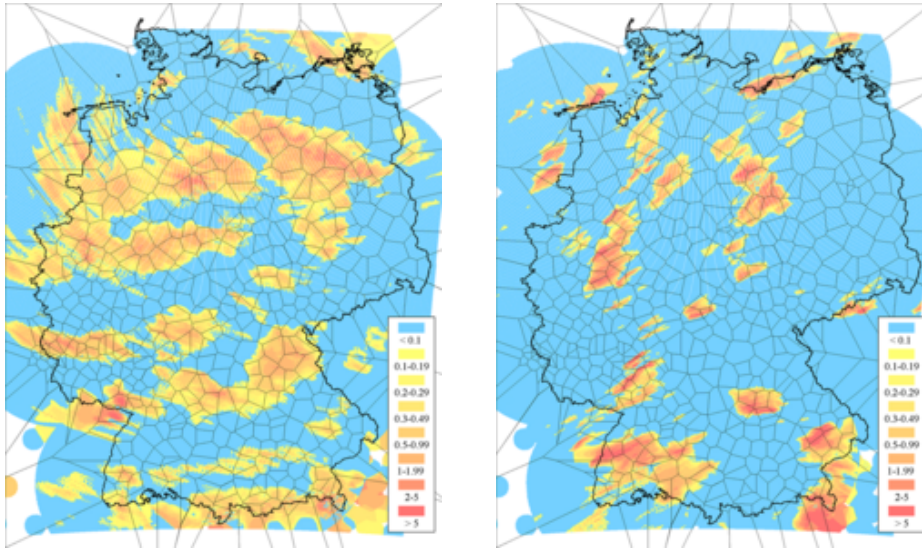


Figure 14: Two radar maps showing data on adjusted hourly precipitation over Germany. Left: sample 1 (with more intensive precipitation); right: sample 2 (with less intensive precipitation).

A crucial question for stochastic modeling is whether the occurrence of precipitation and the resulting amount of precipitation can be modeled independently of each other. Intuitively, this does not seem to be the case, as precipitation amounts appear to be lower at the boundaries of precipitation cells than at their centers. However, precipitation fields are complex meteorological objects and some further justification is desired. Therefore, the tests considered in this paper are applied to adjusted hourly precipitation amounts over Germany obtained from radar measurements. This data was provided by Deutscher Wetterdienst and was used in [12] to validate a stochastic model of area precipitation probabilities. The minimum amount of precipitation observed is 0.1 mm. We consider two samples, labeled 1 and 2, taken at different time points. These are shown in Figure 14.

We treat the samples as realizations of RMCSs. Although we would not, in general, expect these RMCSs to be stationary due to the geographical heterogeneity of Germany, the samples that we have selected appear to justify this assumption. In this setting, the subsampling test is clearly not applicable, as the assumption of isotropy is not satisfied. Thus, we only apply the global rank envelope test.

In order to apply envelope tests to this data, we first estimate  $m$  using the  $k_{\text{mm}}$ -function. For sample 1 we estimate  $\hat{m} = 125$  and for sample 2 we estimate  $\hat{m} = 83$ . Using hexagonal close packings with minimal distances corresponding to the estimates of  $m$  we obtain a  $p$ -value of 0.0007 for sample 1 and a  $p$ -value of 0.001 for sample 2. In both cases, we clearly reject the null hypothesis. Estimates of the mark-weighted  $K$ -function and the  $K$ -function of the random set are shown for sample 2 in Figure 15. Under the null hypothesis, both functions should coincide. Our test reveals that the difference between them is significant. This conclusion is graphically represented by the 95% global rank envelopes (see [17]) in Figure 16. The reason for rejecting the null hypothesis lies in larger values of  $K_{\Gamma}$  than would be expected under the random field model. A similar behavior is observed for sample 1. The results confirm our intuitive suspicion that the precipitation cells and precipitation amounts are not independent. This strongly suggests that, when developing a model for spatial precipitation, amounts should be modeled dependent on the shape and size of the corresponding precipitation cells.

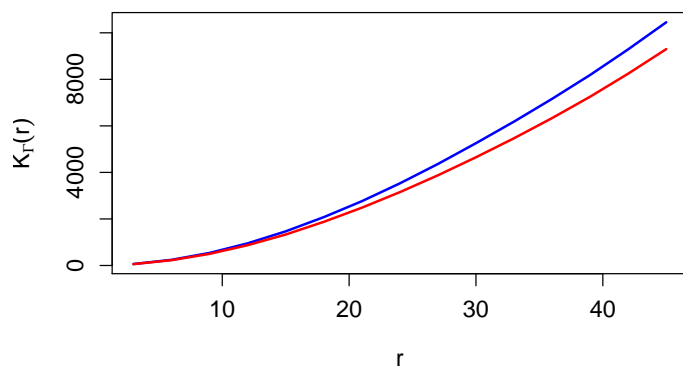


Figure 15: The estimators of mark-weighted  $K$ -function (blue line) and  $K$ -function of the random set (red line) for data sample 2.

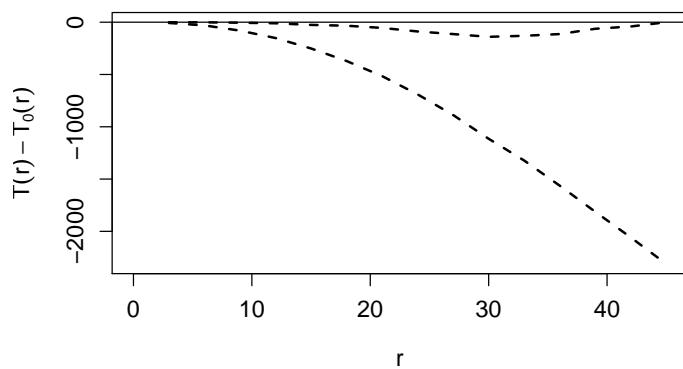


Figure 16: The 95% global rank envelopes (dashed lines) with  $T(r) = \widehat{K}_{\Gamma}(r)$ . For better visualization we subtracted  $T_0(r)$ , the function estimated from data. The horizontal line is outside the envelope which means that the null hypothesis is rejected.

### 5.2. TEM data

In [23], TEM data was used to develop a stochastic model of the 2D nanostructure of a thin polymer:fullerene film, which is a blend of two organic semiconductors. Figure 17 shows two cutouts of the same image. On the

left, the fullerene-rich phase, which is a collection of roughly spherical sets, is shown; on the right, the polymer-rich phase is shown.

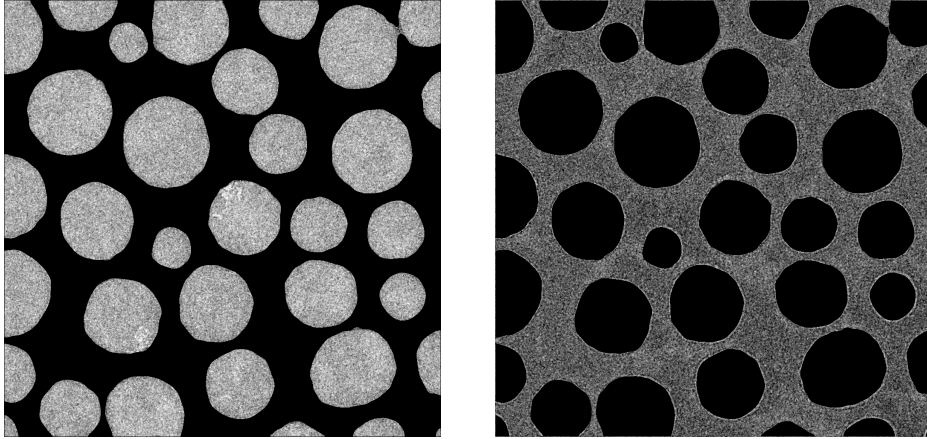


Figure 17: Images extracted from TEM data of the two phases in the polymer:fullerene film. Left: the fullerene-rich phase; right: the polymer-rich phase. Observe the texture present in the image data.

In developing a statistical model for the 2D nanostructure of this material, it is important to use all pertinent information. This includes not just the boundaries between the two phases but also additional information that may be present in the image data. Observe that the images of the two phases in Figure 17 are textured. It is a priori unclear if this texture reveals information about the structure of the material. However, if this is the case, then a stochastic model should endeavor to incorporate this information. Treating the phases as random closed sets and the texture as the marking field, we can apply our testing procedure to determine if the texture is independent of the structure of the phases. In this case, it is reasonable to expect that the RMCS here is both stationary and isotropic; see [23]. The image data is in a  $1024 \times 1024$  pixel window.

We use the global rank envelope test. In both cases, the correlation range of the mark field was estimated to be 85 pixels. Thus, the test points are given by a hexagonal configuration with minimal distance 85. The test does not reject the random field model hypothesis for either the fullerene-rich phase or the polymer-rich phase, with a  $p$ -value of 0.124 for the fullerene-rich phase and a  $p$ -value of 0.727 for the polymer-rich phase. This justifies the modeling approach taken in [23], which did not take the texture observed in

the images into account.

## 6. Conclusion

In this paper, we developed and investigated two non-parametric approaches to testing the random field model hypothesis for RMCSs. These are both based on second order characteristics of RMCSs. The first approach uses a global rank envelope test based on the mark-weighted  $K$ -function. The second approach uses an asymptotic test developed for marked point processes. We carried out extensive simulation studies to assess the performance of these tests. On the basis of these studies, we concluded that the envelope test, using a hexagonal packing for test points, was the better performing of the two tests. Finally, we applied this test to two real world data examples. Based on our results, we suggest the envelope test as a tool for preliminary investigation of data that is being modeled using stationary random marked closed sets. In particular, this test can assist in deciding whether or not to model the marks separately from the random closed set.

There are a number of promising avenues for developing extended versions of our testing approach. For example, it may be possible to extend the approach of this test to non-stationary models by investigating alternative second-order characteristics. In addition, more powerful tests could be developed for specific settings, where the parametric form of the mark field is known (for example, when the mark field is a Gaussian random field).

## Acknowledgements

The authors would like to thank the anonymous referees for their useful comments. This research was supported by the project 7AMB14DE006, funded by the Czech Ministry of Education, Youth and Sports and the German Academic Exchange Service (DAAD). A.K. was supported by the grant SVV-2015-260225.

- [1] G. Ayala and A. Simó. Bivariate random closed sets and nerve fibre degeneration. *Advances in Applied Probability*, 27:293–305, 1995.
- [2] F. Ballani, Z. Kabluchko, and M. Schlather. Random marked sets. *Advances in Applied Probability*, 44:603–616, 2012.

- [3] V. Beneš and J. Rataj. *Stochastic Geometry: Selected Topics*. Kluwer Academic Publishers, Boston, 2004.
- [4] A. Bulinski and E. Spodarev. Central limit theorems for weakly dependent random fields. In E. Spodarev, editor, *Stochastic Geometry, Spatial Statistics and Random Fields*, volume 2068 of *Lecture Notes in Mathematics*, pages 337–383. Springer, Heidelberg, 2013.
- [5] S. N. Chiu, D. Stoyan, W. S. Kendall, and J. Mecke. *Stochastic Geometry and its Applications*. J. Wiley & Sons, Chichester, 3rd edition, 2013.
- [6] N. Cressie. *Statistics for Spatial Data*. J. Wiley & Sons, New York, revised edition, 2015.
- [7] Y. Guan. Tests for independence between marks and points of a marked point process. *Biometrics*, 62:126–134, 2006.
- [8] Y. Guan and D. R. Afshartous. Test for independence between marks and points of marked point processes: a subsampling approach. *Environmental and Ecological Statistics*, 14:101–111, 2007.
- [9] J. Illian, A. Penttinen, H. Stoyan, and D. Stoyan. *Statistical Analysis and Modeling of Spatial Point Patterns*. J. Wiley & Sons, Chichester, 2008.
- [10] E. B. Jensen, K. Kiêu, and H. J. G. Gundersen. On the stereological estimation of reduced moment measures, *Annals of the Institute of Statistical Mathematics*, 42:445–461, 1990.
- [11] A. F. Karr. Inference for stationary random fields given Poisson samples. *Advances in Applied Probability*, 18:406–422, 1986.
- [12] B. Kriesche, R. Hess, B. K. Reichert, and V. Schmidt. A probabilistic approach to the prediction of area weather events, applied to precipitation. *Spatial Statistics*, 12:15–30, 2015.
- [13] B. Kriesche, A. Koubek, Z. Pawlas, V. Benes, R. Hess, and V. Schmidt. A model-based approach to the computation of area probabilities for precipitation exceeding a certain threshold, *Proceedings of the 21st International Congress on Modelling and Simulation*, Gold Coast, Australia, 2103–2109, 2015.

- [14] D. P. Kroese, T. Taimre, and Z. Botev. *Handbook of Monte Carlo Methods*. J. Wiley & Sons, Chichester, 2011.
- [15] I. Molchanov. Labelled random sets. *Theory of Probability and Mathematical Statistics*, 29:113–119, 1984.
- [16] M. Myllymäki, P. Grabarnik, H. Seijo, and D. Stoyan. Deviation test construction and power comparison for marked spatial point patterns. *Spatial Statistics*, 11:19–34, 2015.
- [17] M. Myllymäki, T. Mrkvička, P. Grabarnik, H. Seijo, and U. Hahn. Global envelope tests for spatial processes. *Journal of the Royal Statistical Society: Series B*, to appear.
- [18] D. J. Nott and R. J. Wilson. Multi-phase image modelling with excursion sets. *Signal Processing*, 80:125–139, 2000.
- [19] M. Schlather, P. J. Ribeiro Jr., and P. J. Diggle. Detecting dependence between marks and locations of marked point processes. *Journal of the Royal Statistical Society: Series B*, 66:79–93, 2004.
- [20] J. Staněk, O. Šedivý, and V. Beneš. On random marked sets with a smaller integer dimension. *Methodology and Computing in Applied Probability*, 16:397–410, 2014.
- [21] D. Stoyan and O. Wälder. On variograms in point process statistics, II: Models of markings and ecological interpretation. *Biometrical Journal*, 42:171–187, 2000.
- [22] O. Šedivý, V. Beneš, P. Ponížil, P. Král, and V. Sklenička. Quantitative characterization of microstructure of pure copper processed by ECAP. *Image Analysis & Stereology*, 32:65–75, 2013.
- [23] D. Westhoff, J. J. van Franeker, T. Brereton, D. P. Kroese, R. A. J. Janssen, and V. Schmidt. Stochastic modeling and predictive simulations for the microstructure of organic semiconductor films processed with different spin coating velocities. *Modelling and Simulation in Materials Science and Engineering*, 23:045003, 2015.
- [24] T. Zhang. A Kolmogorov-Smirnov type test for independence between marks and points of marked point processes. *Electronic Journal of Statistics*, 8:2557–2584, 2014.